Title
The thermodynamic stability of intermediate solid solutions in LiFePO 4 nanoparticles

Journal
Journal of Materials Chemistry A, 4(15)

ISSN
2050-7488

Authors
Abdellahi, A
Akyildiz, O
Malik, R
et al.

Publication Date
2016

DOI
10.1039/c5ta10498j

Peer reviewed

Journal of Materials Chemistry A

PAPER

View Article Online
View Journal | View Issue

Cite this: J. Mater. Chem. A, 2016, 4, 5436

The thermodynamic stability of intermediate solid solutions in $LiFePO_4$ nanoparticles

A. Abdellahi,[a] O. Akyildiz,[b] R. Malik,[a] K. Thornton[c] and G. Ceder*[d]

Received 22nd December 2015
Accepted 26th February 2016

DOI: 10.1039/c5ta10498j

www.rsc.org/MaterialsA

Theoretical predictions from first principles and recent advances in *in situ* electrochemical characterization techniques have confirmed the presence of solid-solution states during electrochemical (de)lithiation of $LiFePO_4$ nanoparticles. Surprisingly, however, such thermodynamically unfavorable solid solution states have been observed at rates as low as 0.1C. Given the high diffusivity of Li in $LiFePO_4$ and the thermodynamic instability of homogeneous solid solution states, spinodal decomposition to a thermodynamically favorable two-phase state is expected to occur on time scales as rapid as 1–100 ms. In this paper, we resolve this apparent paradox by demonstrating that, given the symmetry of the low-energy solid-solution Li/Va orderings and the 1D character of Li diffusion, spinodal decomposition from a solid solution preferentially leads to the formation of a diffuse *ac* interface with a large intermediate solid-solution region, as opposed to the commonly assumed *bc* interface. Our first principles predictions not only rationalize the persistence of solid-solution states at low-to-moderate C-rates in high-rate $LiFePO_4$ electrodes, but also explain the observations of large intermediate solid-solution regions at an *ac* interface in single Li_xFePO_4 particles quenched from a high-temperature solid solution.

Introduction

$LiFePO_4$ is an important commercial cathode material for Li-ion batteries due to its safety,[1] reasonable energy density (170 mA h g^{-1}, 3.4 V *vs.* Li/Li^+),[2] and high-rate capability.[3–7] Capacities as high as 130 mA h g^{-1} have been achieved at a 50C rate (where n C corresponds to full (dis)charge in $1/n$ hours), and rates as high as 200C and 400C have been achieved by removing kinetic limitations at the electrode level. These high rates are accessible only when the particle size is reduced to the nano-scale (~50–100 nm), a limitation that has been attributed to reduced Li mobility due to channel-blocking anti-site defects that are present in larger particles.[8–10] However, the mechanism by which pristine nano-sized particles achieve high rates given their equilibrium two-phase behavior ($Li_xFePO_4 \rightarrow xLiFePO_4 + (1-x)FePO_4$) is still an object of debate in the $LiFePO_4$ research community.

Early lithiation models of $LiFePO_4$ single particles predicted lithiation to be initiated by a nucleation event[2,11–14] followed by two-phase growth along the elastically favorable crystallographic *bc* plane.[14,15] However, while nucleation can occur during chemical delithiation due to the high overpotentials associated with the chemical reagents (~1.5 V (ref. 16)), overpotentials in practical electrochemical conditions are much lower and thus unlikely to provide enough driving force to overcome the nucleation barrier required to form the critical nucleus[17] (overpotentials as low as 20 mV are sufficient to cycle entire electrodes[18]).

A solution to the apparent discrepancy between the high-rate capabilities and the two-phase nature of $LiFePO_4$ was first proposed by Malik *et al.*[17,19] Using Density Functional Theory (DFT), the authors identified a non-equilibrium solid-solution pathway accessible at low overpotentials (~30 mV), which circumvents the kinetically prohibitive nucleation step and enables homogeneous lithiation at low overpotentials. Since then, with the development of advanced *in situ* characterization techniques, the presence of solid-solution states during electrochemical (de)lithiation has been experimentally demonstrated. Several *in situ* X-ray diffraction (XRD) experiments have identified lattice parameters intermediate to those of the equilibrium $FePO_4$ and $LiFePO_4$ phases, at (dis)charge rates varying from 0.1C to 60C.[20–23] A recent *in situ* Transmission Electron Microscopy (TEM) experiment has also observed a ~20 nm solid-solution zone in micron-sized $LiFePO_4$ nanowires.[24] It has therefore clearly been established that solid-solution states can play, in various forms, a critical role in the electrochemical (de)lithiation of single $LiFePO_4$ particles.

A key mystery that remains to be elucidated, however, is the persistence of solid-solution states in single particles at low-to-moderate C-rates, (for example, rates in the 0.1–5C range). First principles calculations have indeed shown that homogeneous

[a]Department of Materials Science and Engineering, Massachusetts Institute of Technology, Cambridge, 02141, MA, USA
[b]Department of Materials Science and Engineering, Hitit University, Corum, Turkey
[c]Department of Materials Science and Engineering, University of Michigan, Ann Arbor, 48109, MI, USA
[d]Department of Materials Science and Engineering, University of California, Berkeley, 94720, CA, USA. E-mail: gceder@berkeley.edu

solid-solution states are thermodynamically unfavorable over two-phase coexistence in particles larger than 10 nm.[25,26] Moreover, due to the concave shape of the non-equilibrium solid-solution free energy, homogeneous solid-solution states are unstable with respect to small inhomogeneities in Li concentration. As a particle takes up Li at a fixed current, Li can rapidly diffuse to form a two-phase state inside the particle so as to minimize the particle's free energy. Considering the high diffusivity of Li in $LiFePO_4$ ($D \sim 10^{-8}$ to 10^{-10} cm^2 s^{-1}, from density functional theory[27] and muon-spin relaxation[28] respectively), Li diffusion in a 100 nm particle can occur on time scales as rapid as 1–100 ms, † which is much faster than the typical time required to lithiate a single particle. At 5C, for example, (de)lithiation of a single particle occurs in 720 s, which is much larger than the 1–100 ms time-scales required for phase-separation through Li diffusion. Even correcting for the fact that not all particles are simultaneously active in the electrode (a recent experiment has demonstrated that, at a 5C rate, only ~30% of the particles in an electrode are actively taking up Li at a given time[29]), the time required to (de)lithiate a single particle is still much larger than the time required for phase separation. In summary, while each particle is expected to initiate (de)lithiation through a non-equilibrium solid solution, it remains surprising that homogeneous solid-solution states could persist at low-to-moderate C-rates despite their thermodynamic instability.

In this work, we propose that the persistence of solid-solution states during the (dis)charge of $LiFePO_4$ electrodes at low-to-moderate C-rates is thermodynamic in origin. Using first principles calculations, we demonstrate that spinodal decomposition from a homogeneous solid solution through Li diffusion is more likely to lead to the formation of an *ac* interface, rather than the elastically favored *bc* interface. As a result of the high coherency strain energy associated with a sharp *ac* interface, we further demonstrate that a driving force exists to form a large intermediate solid solution region at the interface, whose dimensions are proportional to the size of the particle (~25–50% of the particle volume depending on the particle morphology). Our results not only rationalize the observation of intermediate lattice parameters at low-to-moderate C-rates in $LiFePO_4$ electrodes, but also explain the observations of stable intermediate solid-solution states at an *ac* interface in single particles quenched from a high-temperature solid solution.[30,31]

Methodology

We consider a single (Li)$FePO_4$ particle which, upon application of under(over)potential (referred to as "overpotential" in the rest of this paper), initiates Li (de)intercalation through the non-equilibrium solid-solution pathway (Fig. 1(a)-(i)). Once the Li concentration surpasses the spinodal point, homogeneous solid-solution states become unstable against infinitesimally small fluctuation in Li concentrations due to the negative curvature of the solid-solution free energy curve in that concentration range (Fig. 1(a)-(ii)). Such inhomogeneities are bound to occur during (dis)charge, as concentration gradients develop at the particle surface due to the applied current. In the presence of such inhomogeneities, uphill Li diffusion occurs from regions of low Li concentration to regions of high Li concentration, leading to phase separation (Fig. 1(a)-(iii)). In practice, the final state of the particle after spinodal decomposition may not involve a sharp interface but rather a diffuse interface. The presence of an intermediate solid-solution region at the interface facilitates the reduction of the coherency strain energy and chemical interfacial energy penalties of a sharp interface at the expense of a higher bulk energy (Fig. 1(b)). The width of the intermediate solid-solution region at thermodynamic equilibrium depends on the ratio between the bulk free energy of the solid solution and the coherency and chemical interfacial energies of the interface orientation that is formed after spinodal decomposition.

In this paper, we determine the free energy and topology (*i.e.* the symmetry of the low energy Li–Va orderings) of the non-equilibrium solid-solution pathway from first principles. Given the topology of the non-equilibrium solid-solution pathway and the 1D character of Li diffusion, we demonstrate that spinodal decomposition from a homogeneous solid-solution state preferentially leads to the formation of an *ac* interface, instead of the commonly assumed *bc* interface. By combining first principles calculations and continuum elasticity, we further demonstrate that a large intermediate solid-solution region at an *ac* interface is thermodynamically favorable over a sharp *ac* interface, as it reduces the high coherency strain energy penalty associated with a sharp *ac* interface. The following paragraphs present this approach in more details.

The free energy of the non-equilibrium solid-solution pathway is estimated by finding the lowest-energy solid-solution configurations that form a topotactic lithiation pathway between $FePO_4$ and $LiFePO_4$. To this end, the energy of a large number of candidate Li–Va orderings is calculated within the Generalized Gradient Approximation (GGA(PBE)+U) to density functional theory (DFT), as implemented in the Vienna Ab Initio Simulation Package (VASP). A self-consistent U value for Fe of 4.3 is used,[32] with an energy cutoff of 520 eV and a *k*-points spacing of 0.15 A^{-1} (equivalent to a $4 \times 8 \times 12$ mesh for a structure containing one unit cell). All calculations are performed in the ferromagnetic state, following previous studies.[33]

The driving force to form an intermediate solid-solution region at a $LiFePO_4/FePO_4$ interface is calculated using the setup illustrated in Fig. 1(b). Three regions are defined in the particle: a $LiFePO_4$ region, a $FePO_4$ region and a Li_xFePO_4 solid-intermediate solution region (ISSR) with volume fraction y_{ISSR}. The free energy penalty to form a sharp interface ($y_{ISSR} = 0$) is the sum of its coherency strain energy and chemical interfacial energy penalties:

$$F_{\text{sharp boundary}} = Ve_{\text{strain}}^{\text{sharp boundary}} + A\gamma \quad (1)$$

where V is the particle volume, $e_{\text{strain}}^{\text{sharp boundary}}$ is the volume-averaged coherency strain energy density (total strain energy in the particle divided by the total volume of the particle) in the

† These values were obtained using Fickian scaling $t \sim r^2/D$, with the theoretical and experimental values of D provided above.

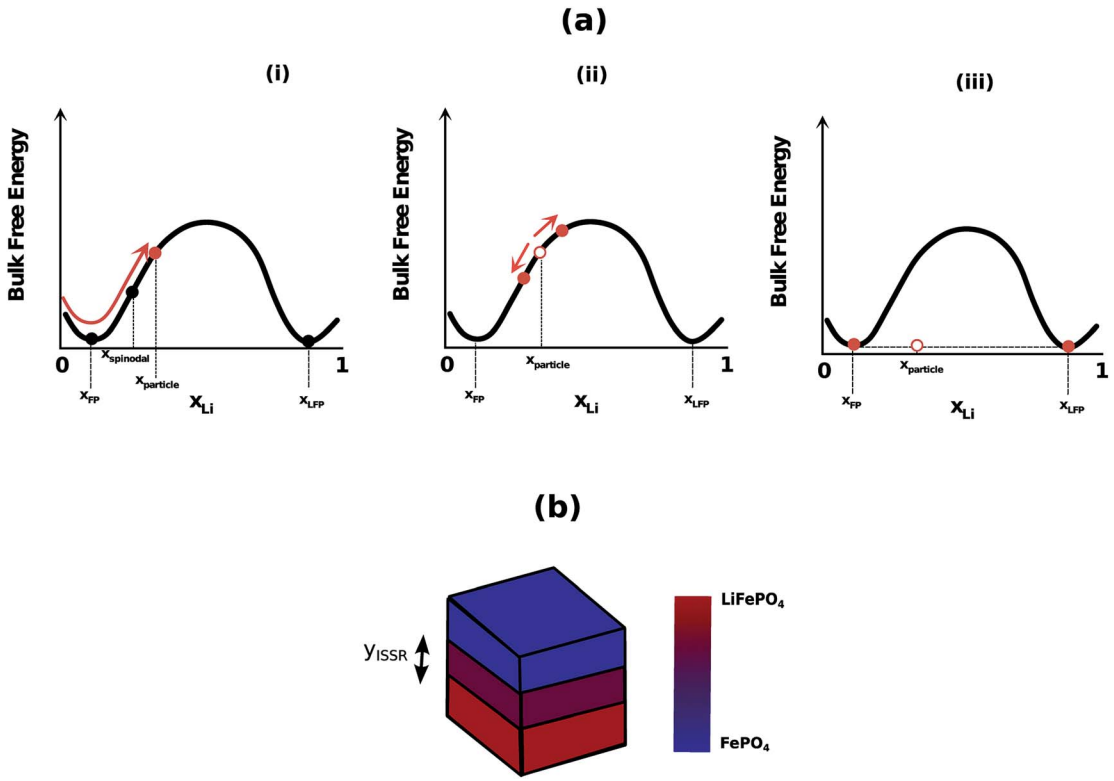

Fig. 1 (a) Particle initiating lithiation through a non-equilibrium solid-solution pathway and subsequently relaxing to a two-phase state. (b) The final state after spinodal decomposition consists in a $LiFePO_4$ region, a $FePO_4$ region, and potentially an intermediate solid-solution region (ISSR), with a volume fraction y_{ISSR}.

particle resulting from a sharp interface, A is the interfacial area and γ is the chemical interfacial energy per unit area.

The free energy penalty for the creation of a diffuse interface is the sum of the bulk free energy of the ISSR, the coherency strain energy resulting from the presence of a diffuse interface and the gradient energy penalty in the ISSR:

$$F_{\text{diffuse boundary}} = V y_{\text{ISSR}} \overline{f}_{\text{solid-solution}} + V e_{\text{strain}}^{\text{diffuse boundary}} + \int_{V_{\text{ISS}}} k|\nabla x_{\text{Li}}|^2 \mathrm{d}V \quad (2)$$

where y_{ISSR} is the volume fraction of the ISSR, $\bar{f}_{\text{solid-solution}}$ is the volume-averaged bulk free energy density in the ISSR, $e_{\text{strain}}^{\text{diffuse boundary}}$ is the volume-averaged coherency strain energy density in the particle resulting from a diffuse boundary, κ is the gradient energy coefficient and ∇x_{Li} is the concentration gradient in the ISSR. The difference in free energy between a diffuse interface and a sharp two-phase boundary ($y_{\text{ISSR}} = 0$) is obtained by taking the difference between eqn (2) and (1):

$$F_{\text{diffuse boundary}} - F_{\text{sharp boundary}} = V y_{\text{ISSR}} \overline{f}_{\text{solid-solution}} + V\left(e_{\text{strain}}^{\text{diffuse boundary}} - e_{\text{strain}}^{\text{sharp boundary}}\right) + \left(\int_{V_{\text{ISSR}}} k|\nabla x_{\text{Li}}|^2 \mathrm{d}V - A\gamma\right) \quad (3)$$

The first term represents the bulk free energy penalty to form the ISSR (positive), the second represents the decrease in coherency strain energy in forming a diffuse interface (negative) and the third term represents the decrease in chemical interfacial energy in forming a diffuse interface (negative). The range of y_{ISSR} for which $F_{\text{ISS}} - F_{\text{sharp boundary}}$ is negative constitutes the range of ISSR volume fraction for which intermediate solid solutions are thermodynamically favorable over a sharp interface. The equilibrium thermodynamic value of y_{ISSR} (valid in the limit of zero rates) can be evaluated by minimizing eqn (3) with respect to y_{ISSR}. This equilibrium value is denoted by $y_{\text{ISSR,eq}}$.

Coherency strain energy values for the sharp boundary and diffuse boundary cases are calculated by numerically solving the equation of continuum elasticity for coherent interfaces under a traction-free boundary condition, as described elsewhere.[26] Chemical interfacial energies are taken from the first principles evaluations of Abdellahi *et al.*,[26] and the associated gradient energy penalty term is calculated from the well-known relation:[34]

$$\kappa = \frac{\gamma^2 \underline{\Omega}_{\text{Li}}}{\underline{f}_{\text{solid-solution}}} \quad (4)$$

where γ is the chemical interfacial energy per unit area, $\underline{\Omega}_{\text{Li}}$ the volume per formula unit of Li and $\underline{f}_{\text{solid-solution}}$ is the average value of the solid-solution free energy (per formula unit of Li) in the $x_{\text{Li}} = [0,1]$ concentration range.

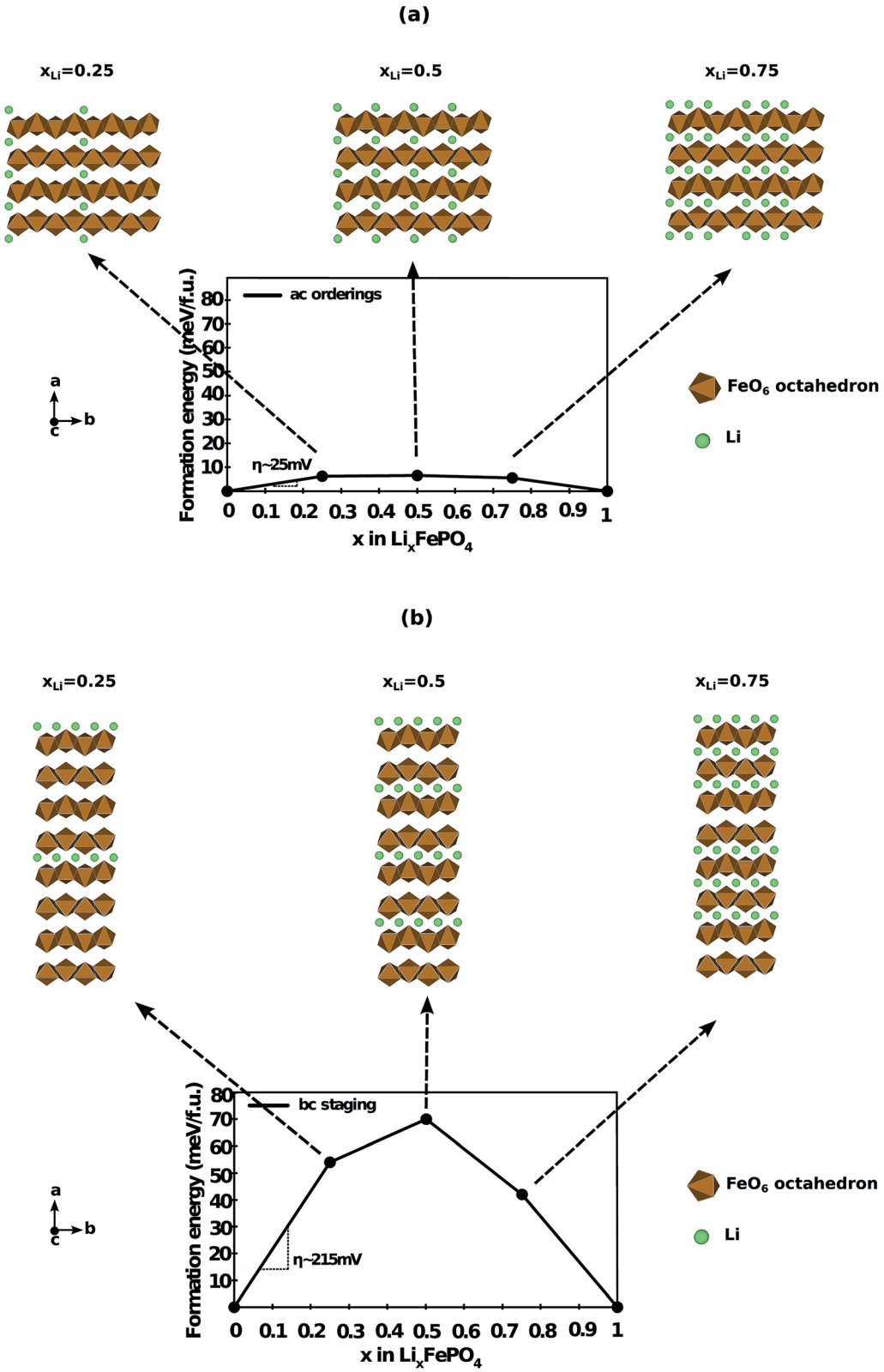

Fig. 2 Low-energy orderings in the non-equilibrium solid-solution pathway in Li_xFePO_4, as determined by density functional theory. (a) The non-equilibrium solid-solution pathway in Li_xFePO_4 is governed by the energetics of *ac* orderings (alternately lithiated/delithiated *ac* planes in proportion to the Li concentration) and is accessible at low overpotentials (~25 mV). (b) In comparison, previously reported *bc* staging configurations can only be accessed at high overpotentials (~215 mV).

Results

Fig. 2(a) shows the low-energy solid-solution orderings identified using density functional theory. At each concentration, the lowest energy solid-solution states are comprised of a periodic arrangement of lithiated and delithiated *ac* planes, in proportion to the lithium concentration (for example, at $x_{Li} = 0.5$, one out of two *ac* planes is lithiated). In these low-energy solid-solution states, each *b*-channel in the particle is partially lithiated, contrarily to the channel-by-channel lithiation often assumed in the literature.[14,19] The maximum energy of these low-energy states is ~6 meV per formula unit (meV per f.u.), in agreement with the 700 J mol^{-1} (7 meV per f.u.) solid-solution mixing enthalpy obtained by Dodd *et al. via* Differential Scanning Calorimetry.[16] The overpotential required to access this solid-solution pathway can be estimated by taking the derivative $dE_{formation}/dx_{Li}$ at $x_{Li} = 0$, yielding a zero-rate overpotential of 25 mV. This overpotential is consistent with the low ~10 mV hysteresis measured in slow cycling of $LiFePO_4$ electrodes.[18] Note that the low-energy solid solution *ac* orderings identified using DFT are in agreement with independent predictions using a previously developed cluster expansion for Li_xFePO_4.[17,33]

While the low-energy non-equilibrium solid-solution pathway (dominated by *ac* orderings) has a low bulk free energy, homogeneous solid-solution states are still thermodynamically unfavorable over two-phase coexistence in a single particle, even when the coherency strain energy and chemical interfacial energy penalties are considered. This is true for both a sharp *bc* interface (the elastically favorable interface orientation) and a sharp *ac* interface (which is observed in quenching experiments of Li_xFePO_4 solid solutions[30]). In the case of a cubic particle, the volume-averaged coherency strain energy density is ~1.7 meV per f.u. for the *bc* interface and ~3 meV per f.u. for the *ac* interface (note that, as will be seen later in the text, most of the coherency strain energy is localized in the vicinity of the interface).[26] In both cases, the coherency strain energy is lower than the 6 meV per f.u. bulk free energy of homogeneous solid-solution states. This is illustrated in Fig. 3. Note that the additional effect of chemical interfacial energy penalty at typical ~100 nm particle sizes is small (on the order of 0.5 meV per f.u. for a *bc* interface and 0.03 meV per f.u. for an *ac* interface) and does not change the conclusion.[26]

In principle, spinodal decomposition can therefore lead to relaxation to either a *bc* interface or to an *ac* interface, with the *bc* interface being generally thermodynamically favorable in a finite particle by virtue of its lower coherency strain energy (by ~1.3 meV per f.u. at the particle scale). But while a driving force exists to form both interface orientations, the topology of the non-equilibrium solid-solution pathway, coupled with the constraint of 1D diffusion along the *b* direction, suggests that relaxation to an *ac* interface is much more likely. During the spinodal decomposition process, each region in the particle must indeed be dominated by local *ac* orderings in order for the bulk free energy to continuously decrease across the particle. With Li diffusion largely one-dimensional along the *b* direction, the continuous spinodal decomposition process is most likely to lead to the formation of an *ac* interface, as illustrated in Fig. 4(a)–(c). Although the *bc* interface is the thermodynamically favorable interface, relaxation to a *bc* interface requires significant diffusion in the *a* and *c* directions (Fig. 4(d)), which is much slower than diffusion in the *b* direction (even with 1% Li–Fe antisite defect in the particle, D_b is larger than D_a and D_c by a factor of 1000 (ref. 10)). Moreover, relaxation to a *bc*-interface from an *ac* ordering can only occur at the expense of an initial increase in bulk free energy, since the symmetry of *ac* orderings must be broken locally (from *b*-channels being partially lithiated to some *b*-channels being fully lithiated and others being fully delithiated).

This prediction is consistent with the quenching experiment of Chen *et al.* (Fig. 5).[30] In this experiment, $LiFePO_4$ particles are chemically delithiated to $Li_{0.6}FePO_4$, producing a series of *bc* interfaces inside the particle (presumably through nucleation and growth, owing to the high overpotentials induced by chemical reagents[16]). After heating to $T \sim 200$ °C, a homogeneous, thermodynamically favorable solid-solution state is formed within the particle, through slow-Li diffusion along the *a* direction. After quenching to room temperature, at which homogeneous solid-solution states are thermodynamically

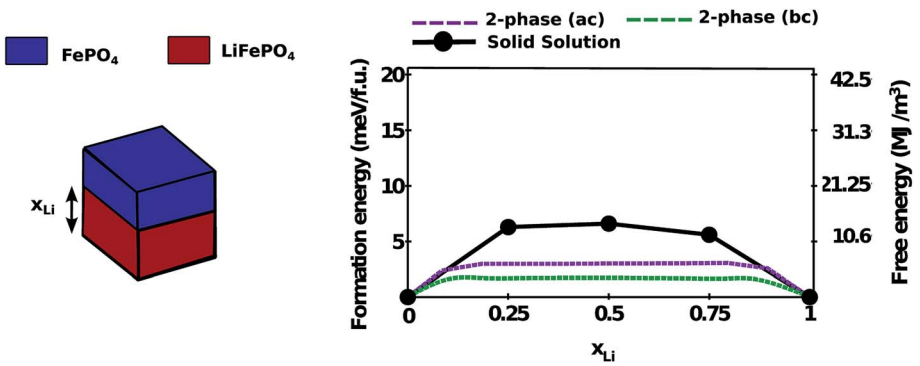

Fig. 3 Comparing the free energy of a homogeneous solid solution with respect to the free energy of phase-separation to a sharp *bc* or *ac* interface at different Li concentrations. Since the effect of chemical interfacial energy is small for typical ~100 nm particles (0.5 meV per f.u. for a *bc* interface and 0.03 meV per f.u. for an *ac* interface), only the contribution of coherency strain energy to the energy penalty of phase-separation is considered.

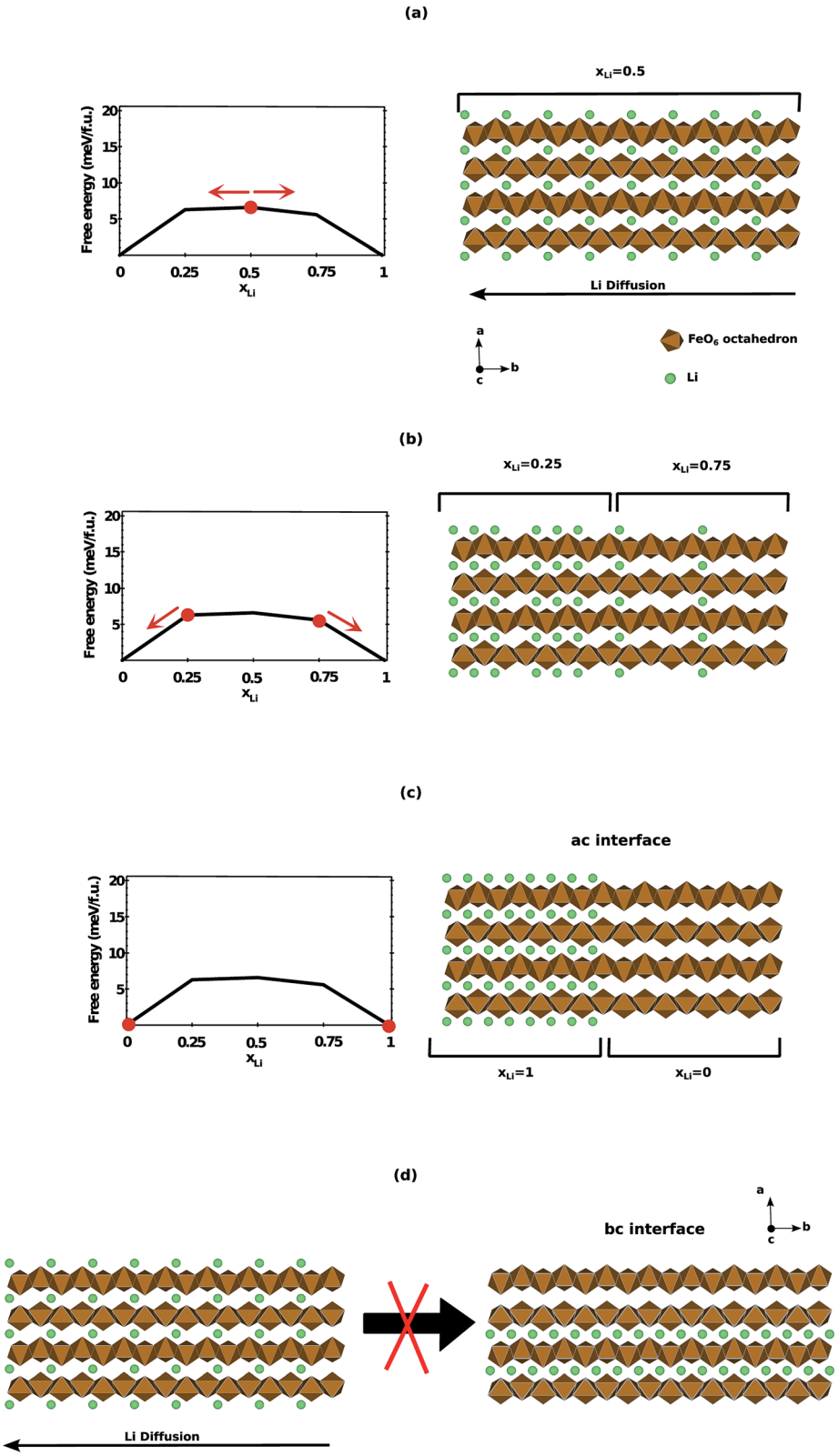

Fig. 4 Orientation of the most likely interface after spinodal decomposition. (a)–(c) Spinodal decomposition from a homogeneous solid-solution dominated by *ac* orderings through 1D Li diffusion along the *b* direction preferentially leads to the formation of an *ac* interface. (d) Spinodal decomposition from a homogeneous solid-solution state to a *bc* interface is unlikely, as it requires an initial increase in the local bulk free energy (through the breaking of local *ac* orderings), as well as significant diffusion in the *a* and *c* directions (several order of magnitudes lower than in the *b* direction).

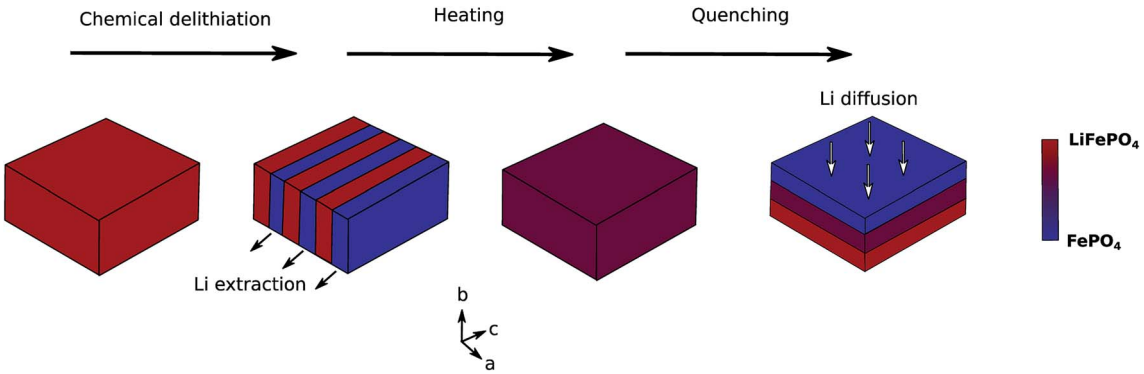

Fig. 5 Illustration of the quenching experiment by Chen *et al.*[30]

unfavorable, spinodal decomposition occurs through Li diffusion in the *b* direction. This leads to the formation of an *ac* interface with a large intermediate solid-solution region at the interface, consisting in one or more intermediate phases. This intermediate solid-solution region is found to be indefinitely stable (stability longer than 5 months). The experiment yielded similar results for large *ac*-platelet particles (2 μm × 200 nm × 4 μm) and intermediates-sized near-cubic particles

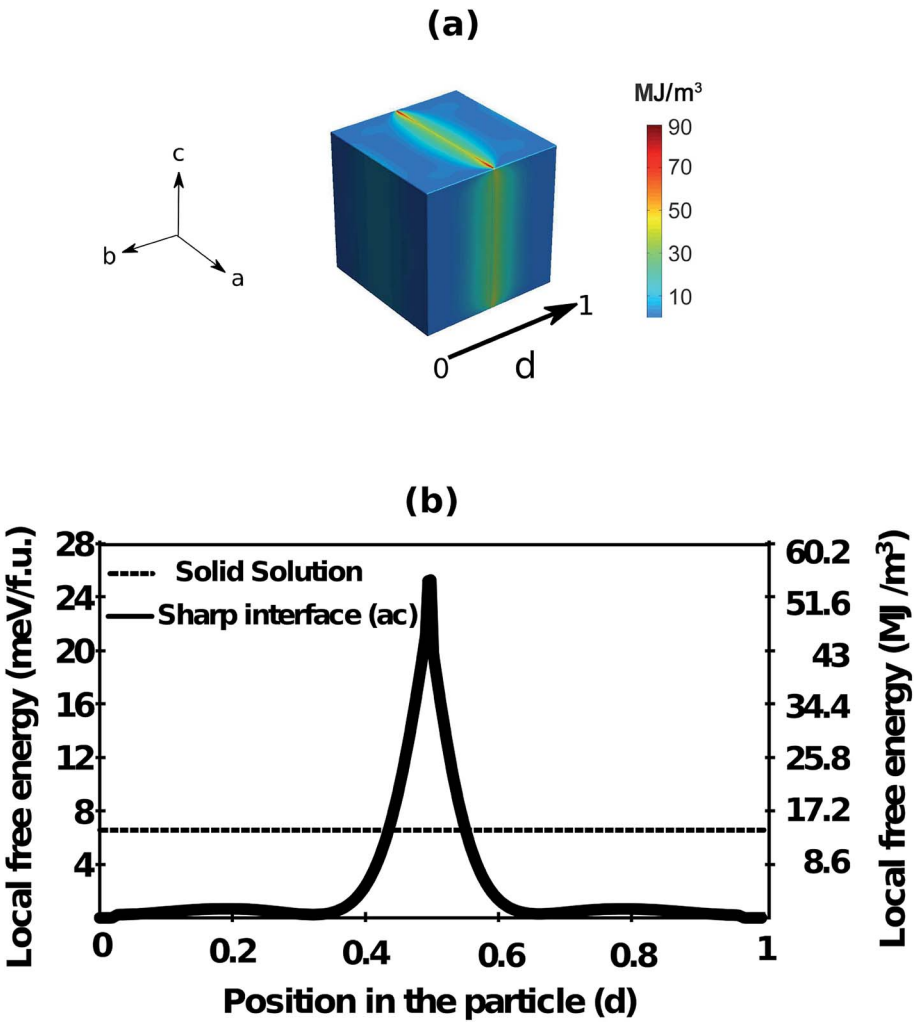

Fig. 6 Comparing the local free energy distribution of a homogeneous solid-solution state and of a sharp *ac* interface. In both cases, the Li concentration is set to $\bar{x}_{Li} = 0.5$ at the particle level. (a) Contour plot of the coherency strain energy density profile resulting from a sharp *ac* interface, and (b) the local coherency strain energy density at different positions in the particle is compared with the non-equilibrium solid-solution free energy (line scan along the *b* direction, at 80% of the distance between the particle center and the external *bc* surface).

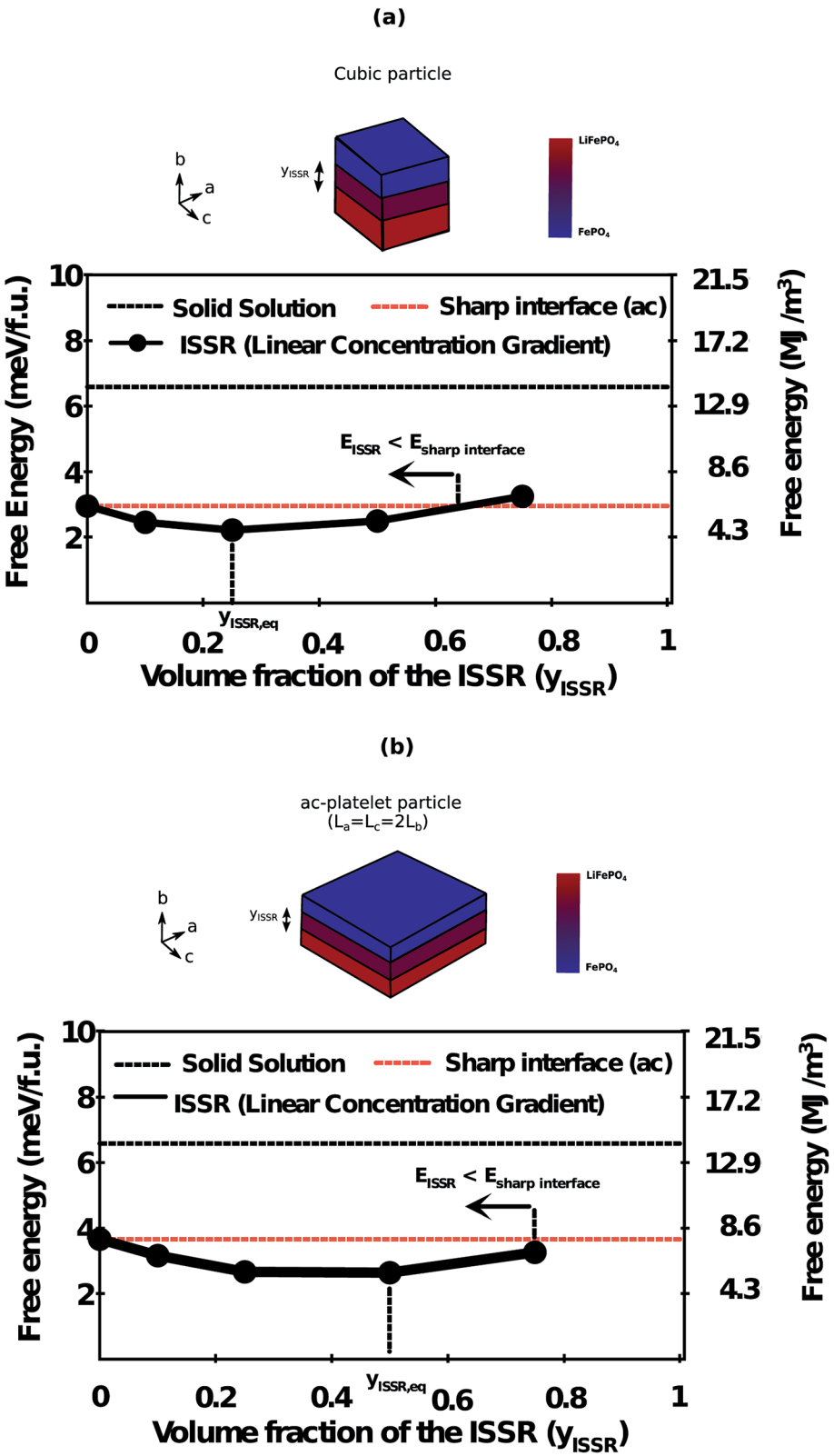

Fig. 7 Thermodynamic stability of intermediate solid-solution states after spinodal decomposition to an *ac* interface. The energy penalty for a sharp interface and for a diffuse ISSR interface (averaged over the entire particle) are compared, as a function of the volume fraction of the ISSR (y_{ISSR}), for (a) a cubic particle and (b) an *ac*-platelet particle (aspect ratios $L_b/L_a = L_b/L_c = 0.5$). For a cubic particle, an ISSR is thermodynamically favorable of a sharp interface for $y_{ISSR} < 50\%$. The corresponding volume fraction is $y_{ISSR} < 75\%$ for an *ac*-platelet particle. The equilibrium value of y_{ISSR} (value of y_{ISSR} for which the total free energy is minimized) is $y_{ISSR,eq} = 25\%$ for a cubic particle and $y_{ISSR,eq} = 50\%$ for an *ac*-platelet particle.

(300 nm × 200 nm × 500 nm). Therefore, both our first principles predictions and the quenching experiment of Chen *et al.*[30] demonstrate that no easily accessible topotactic pathway exists for a particle to continuously relax from a homogeneous solid solution to a *bc* interface, despite the *bc* interface generally being the thermodynamically favorable interface.[26]

An *ac* interface is therefore most likely to be formed after spinodal decomposition from a solid solution, and, on average over the entire particle, is thermodynamically favorable over a homogeneous solid solution. However, further investigations reveal that a diffuse *ac* interface with a large intermediate solid solution is thermodynamically favorable over a sharp *ac* interface. A closer inspection of the coherency strain energy profile in the particle reveals that, near the interface, the coherency strain energy is significantly higher than the solid-solution free energy. This is shown in Fig. 6. Fig. 6(a) shows a contour map of the coherency strain energy density in a cubic particle containing an *ac* interface (average Li concentration of $\bar{x}_{Li} = 0.5$), and Fig. 6(b) shows the profile of the coherency strain energy in the particle interior along the direction perpendicular to the interface. The coherency strain energy at the vicinity of the interface is found to be on the order 25 meV per f.u., which is significantly higher than the ~6 meV per f.u. bulk free energy of the solid solution. (Note that, for an *ac* interface, the effect of the chemical interfacial energy is small (0.03 meV per f.u. for a 100 nm particle) and can be neglected[26]).

Based on these energy scales, introducing an ISSR at the $LiFePO_4/FePO_4$ interface can decrease the free energy of the particle by reducing the coherency strain energy in the vicinity of the interface. This is illustrated quantitatively in Fig. 7, in which the free energy resulting from the insertion of an ISSR at the $LiFePO_4/FePO_4$ interface (normalized by the particle volume) is plotted with respect to the ISSR volume fraction y_{ISSR} (a concentration of $\bar{x}_{Li} = 0.5$ at the particle level is assumed). A uniform concentration gradient in the ISSR is considered (from $x_{Li} = 1$ to $x_{Li} = 0$). In Fig. 7(a), the analysis is made for a cubic particle, and in Fig. 7(b), the analysis is made for an *ac*-platelet particle with an aspect ratio of 2 ($L_a/L_b = L_c/L_b = 2$, where L_a, L_b and L_c are the particle dimensions along the *a*, *b* and *c* directions respectively). Such *ac*-platelet morphologies, for which the particle dimension along the *b* direction is smaller than along the *a* and *c* dimensions, are common in the $LiFePO_4$ literature.[15,30,35,36] For a cubic particle (Fig. 7(a)), it is found that ISSR volume fractions as high as 50% are thermodynamically favorable over a sharp interface, with an equilibrium volume fraction ($y_{ISSR,eq}$) of 25%. For *ac*-platelet particles with an aspect ratio of two (Fig. 7(b)), the volume fraction of thermodynamically favorable intermediate solid-solution states is larger than in the cubic particle, due to the larger coherency-strain energy at the interface (since the *ac* cross section is larger in proportion to other cross sections).[26,37] For such particles, an ISSR volume fraction of up to ~75% of the particle volume is favorable over a sharp *ac* interface, with an equilibrium volume fraction of $y_{ISSR,eq} \approx 50\%$. While the analysis of Fig. 7 was performed for a particle-level Li concentration of $\bar{x}_{Li} = 0.5$, large intermediate solid solution regions are also expected at other Li concentrations, as the coherency strain energy resulting from a sharp interface is largely independent of Li concentration in a wide concentration range ($\bar{x}_{Li} \in [0.1,0.9]$ in cubic particles).[26]

At a given particle morphology, coherency strain energy scales as the volume of the particle. Because the thermodynamic stability of intermediate solid solutions originates from a reduction in coherency strain energy, the equilibrium volume fraction of the ISSR (at a given Li concentration) is therefore independent of the particle size for a given particle morphology. For example, with $y_{ISSR,eq}$ being ~25% for a cubic particle (at $\bar{x}_{Li} = 0.5$), a 50 nm cubic particle is predicted to have a 12.5 nm-thick ISSR at thermodynamic equilibrium while a 100 nm cubic particle is predicted to have a 25 nm-thick ISSR at thermodynamic equilibrium. The ISSR volume fraction and thickness increase for platelet particles with larger (010) faces, which are common in the $LiFePO_4$ literature.

Our results therefore indicate that, while spinodal decomposition from a homogeneous solid solution can rapidly occur at the particle surface due to fast Li diffusion, it is more likely to lead to a diffuse *ac* interface with an intermediate solid-solution region occupying a large fraction of the particle volume (~25–50% for the particle morphologies illustrated in Fig. 7). Moreover, this volume fraction is independent of the particle size at a given particle morphology. This result explains not only the persistence of intermediate solid-solution states at an *ac* interface after quenching of homogeneous solid solutions, but also the observation of intermediate lattice parameters during *in situ* XRD (dis)charging experiments at low-to-moderate C-rates.

Discussion

An important consequence of our study is that there exists a thermodynamic origin to the persistence of large intermediate solid solutions region during (de)lithiation. Even in the limit of zero-rates, particle-by-particle lithiation[18] is predicted to occur through the non-equilibrium solid-solution pathway, followed by spinodal decomposition to a two-phase state with a large intermediate solid-solution region. In agreement with this finding, *in situ* TEM experiments have observed intermediate solid-solution states at rates as low as 5C,[24] and a recent *in situ* XRD experiment has observed intermediate solid solution states at rates as low as 0.1C (~20% of the particle volume).[23] The fact that intermediate lattice parameters are generally not observed at very low C-rates by experimental methods relying on electrode-level measurements can be ascribed to the multi-particle behavior of $LiFePO_4$.[38,39] In the low-rate limit, particles transform sequentially while at high rates, they transform in parallel. High rates allow more particles to transform simultaneously, producing sufficiently large intensity in diffraction peaks at intermediate lattice parameters.

While some *in situ* XRD experiments have identified a continuum spectrum of intermediate lattice parameters in the electrode,[22] others have measured discrete peaks that have been attributed to one or several discrete intermediate phases.[20] In agreement with the latter observation, our calculations predict that large intermediate solid solution regions made of discrete intermediate phases are also thermodynamically favorable over a sharp interface. An ISSR containing a single intermediate phase, for example, has an equilibrium ISSR volume fraction of

$y_{ISSR,eq} = 10\%$ (cubic particle, $\bar{x}_{Li} = 0.5$ at the particle level). This percentage rises to 25% for the *ac*-platelet particle illustrated in Fig. 7(b). In general, however, having multiple intermediate phases in the ISSR is energetically favorable over a single intermediate phase, as it further reduces both the coherency strain energy in the particle and the bulk free energy penalty of the ISSR (as phases closer in concentration to the equilibrium phases have a lower bulk free energy).

Intermediate lattice parameters are typically measured in nano-sized particles and not in micron-sized particles.[40] Because an ISSR reduces the high coherency strain energy resulting from a sharp interface, and because coherency strain energy scales with particle volume, the formation of an ISSR is thermodynamically favorable over a sharp coherent interfaces at all particle sizes. In large particles, however, formation of a semicoherent interface, where the lattice misfit is accommodated to some degree by interfacial dislocations, is even more favorable. A semicoherent interface reduces the coherency strain energy penalty (which scales as the particle volume) at the expense of a higher chemical interfacial energy (which scales as the interfacial area), through the formation of misfit dislocations. This process is favorable in large particles due to their small interfacial-area-to-volume ratios. Supporting the hypothesis that the formation of misfit dislocations is responsible for the lack of ISSR in large particles, the propagation of a semi-incoherent *ac* interface with a large density of dislocations was observed during an *in situ* lithiation experiment of micron-sized $FePO_4$ particles.[41] Rate capabilities were found to be low (1C rate at a ~400 mV overpotential), indicating that the presence of interfacial dislocations significantly affects interfacial mobility.

Overall, the existence of a low-energy non-equilibrium solid-solution pathway in $LiFePO_4$ has multiple benefits. First, the existence of a non-equilibrium low-energy solid-solution pathway allows particles to initiate (de)lithiation at low overpotentials, increasing rate capabilities with respect to systems undergoing nucleation and growth. Moreover, after spinodal decomposition, the presence of a thermodynamically favorable ISSR at the interface leads to a decrease in coherency strain energy. This in turn reduces mechanical damage upon cycling and improves cyclability. Finally, the presence of an ISSR decreases the driving force to form a semicoherent interface, thus enhancing cyclability and rate capabilities.

It is important to note that our model operated under the assumption that (de)lithiation is always initiated by the low-energy non-equilibrium solid-solution pathway, which is dominated by low-energy *ac* orderings and accessible at low overpotentials. However, when higher overpotentials are applied, more lithiation pathways may become available. Nucleation and growth, for example, can occur in the large overpotential limit. This is the case during chemical delithiation, where large applied overpotentials (~1.5 V (ref. 16)) can lead to nucleation and subsequent formation of the elastically favorable sharp *bc* interface. Given the low coherency strain energy at a sharp *bc* interface, the formation of an intermediate solid-solution region is largely dominated by the chemical interfacial energy. Using the well-known relation $\delta = \sqrt{\kappa/\bar{f}_{\text{solid-solution}}}$ (ref. 34) (where δ is the interfacial width, $\bar{f}_{\text{solid-solution}}$ is the average solid-solution free energy density (per unit volume) in the $x_{Li} = [0,1]$ range and κ is the gradient energy coefficient of the *bc* interface[26]), the size of the intermediate solid-solution region is found to be ~10 nm regardless of the particle size. This prediction is consistent with *ex situ* observations of chemically delithiated particles[15,36] and further

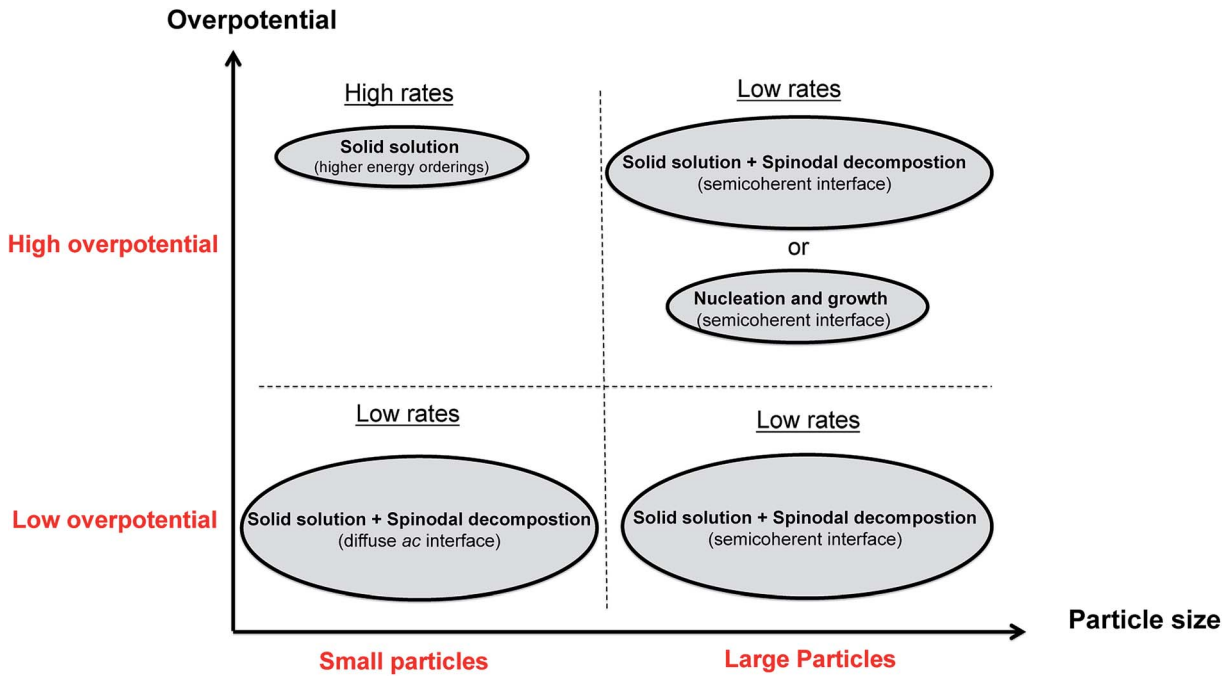

Fig. 8 Qualitative map of the lithiation mechanism in $LiFeO_4$ single particles as a function of particle size and applied overpotential. Note that this map applies to the particles that are actively transforming in the electrode.

confirms that the formation of a *bc* interface is not the dominant mechanism during electrochemical delithiation of nanoparticles. The ~10 nm ISSR associated with the formation of a *bc* interface is indeed inconsistent with *in situ* XRD measurements on ~186 nm particles, where the solid solution region was found to be on the order of the particle size.[22]

High-energy solid-solution pathways, different from the low energy *ac* orderings reported in this paper, can also be accessed if the applied overpotential is large enough. The experimentally observed "*bc* staging" ordering,[42–45] which consists of a solid solution of alternately lithiated *bc* planes, is one such example. Staging configurations were observed in *ex situ* conditions in the form of a small ~2 nm ISSR[43] or uniformly throughout nanoparticles or micron-sized nanowires.[44] DFT calculations demonstrate that the energy required to access the *bc* staging pathway is significantly higher than the energy required to access the *ac* ordering pathway (70 meV per f.u [in agreement with the values found by Sun *et al.*[45]], instead of 6 meV per f.u at $x_{Li} = 0.5$). The overpotential to access the *bc*-staging pathway, which can be calculated from $dE_{formation}/dx_{Li}$ at dilute staging concentrations, is also significantly higher (~215 mV instead of ~25 mV, as shown in Fig. 2(b)). The *bc*-staging pathway therefore cannot account for the high-rate capability of $LiFePO_4$, which is defined as the ability to achieve high currents at low overpotentials, but could become competitive with the low energy *ac* solid-solution pathway at large overpotentials. Once a uniform *bc* staging configuration is formed in a particle, it is likely to remain metastable, as relaxation from a *bc* staging requires significant Li diffusion in the slow-diffusing *a* direction. This may explain observations of uniform *bc* staging throughout nanoparticles and micron-sized nanowires.[44]

Fig. 8 summarizes the above considerations by qualitatively illustrating the range of possible lithiation mechanisms in $LiFePO_4$ particles as a function of the particle size and applied overpotential. At low overpotentials, both small and large particles initiate lithiation *via* the non-equilibrium solid solution pathway, dominated by low energy *ac* orderings. Spinodal decomposition in small particles preferentially leads to the formation of a diffuse *ac* interface, while it leads to the formation of a semicoherent interface in large particles. At high overpotentials, small particles can access higher energy orderings in the solid solution (such as the *bc* staging configuration). The higher rates induced by these high overpotentials also lead to a higher retention of the solid solution. In large particles, higher overpotentials open up the nucleation and growth pathway (due to the large number of nucleation sites), in addition to the spinodal decomposition pathway. Both mechanisms, however, lead to low rates due to poor Li diffusivity in large particles, through the presence of channel-blocking antisite defects[10] and the formation of semicoherent interfaces.

Conclusion

In this paper, we resolved the apparent paradox between the high Li diffusivity in $LiFePO_4$ and the persistence of thermodynamically unstable solid-solution states during (dis)charge at low to moderate C-rates. Using a combination of first principles calculations and continuum elasticity, we demonstrated that, even under rate conditions such that relaxation to a two-phase state is kinetically possible, the thermodynamically favorable state in a single particle is not a sharp interface but rather a diffuse interface with an intermediate solid-solution region that occupies a significant fraction of the particle volume. Our results not only explain the persistence of solid-solution regions at low to moderate C-rates in $LiFePO_4$ electrodes, but also explain the observations of stable intermediate solid-solution states at an *ac* interface in single particles quenched from a solid solution.

Acknowledgements

This work was supported as part of the NorthEast Center for Chemical Energy Storage (NECCES), an Energy Frontier Research Center funded by the U.S. Department of Energy, Office of Science, Basic Energy Sciences under Award #DE-SC0012583. High performing computing resources were provided by the Extreme Science and Engineering Discovery Environment (XSEDE), which is supported by National Science Foundation Grant Number OCI-1053575, under allocations TG-DMR97008S and TG-DR110007. The authors would like to acknowledge Bernardo Orvananos and Hui-Chia Yu for helpful comments and discussions. O. Akyildiz acknowledges support from the Turkish Scientific and Technical Research Council, TUBITAK, through BIDEB 2219 Program and Grant No. 113F091.

References

1 K. Zaghib, A. Mauger, J. B. Goodenough, F. Gendron and C. M. Julien, Electronic, Optical, and Magnetic Properties of $LiFePO_4$: Small Magnetic Polaron Effects, *Chem. Mater.*, 2007, **19**, 3740–3747.
2 A. Padhi, K. Nanjundaswamy and J. Goodenough, Phospho-olivines as positive-electrode materials for rechargeable lithium batteries, *J. Electrochem. Soc.*, 1997, **144**, 1188–1194.
3 H. Huang, S. C. Yin and L. F. Nazar, Approaching Theoretical Capacity of $LiFePO_4$ at Room Temperature at High Rates, *Electrochem. Solid-State Lett.*, 2001, **4**, A170.
4 A. Yamada, S. C. Chung and K. Hinokuma, Optimized $LiFePO_4$ for Lithium Battery Cathodes, *J. Electrochem. Soc.*, 2001, **148**, A224.
5 C. Sides, F. Croce, V. Young, C. Martin and B. Scrosati, A high-rate, nanocomposite $LiFePO_4$/carbon cathode, *Electrochem. Solid-State Lett.*, 2005, **8**, A484–A487.
6 A. Yamada, M. Yonemura, Y. Takei, N. Sonoyama and R. Kanno, Fast charging $LiFePO_4$, *Electrochem. Solid-State Lett.*, 2005, **8**, A55–A58.
7 B. Kang and C. Gerbrand, Battery materials for ultrafast charging and discharging, *Nature*, 2009, **458**, 190–193.
8 M. S. Islam, D. J. Driscoll, C. A. J. Fisher and P. R. Slater, Atomic-Scale Investigation of Defects, Dopants, and Lithium Transport in the $LiFePO_4$ Olivine-Type Battery Material, *Chem. Mater.*, 2005, **17**, 5085–5092.

9 S.-Y. Chung, S.-Y. Choi, T. Yamamoto and Y. Ikuhara, Atomic-Scale Visualization of Antisite Defects in $LiFePO_4$, *Phys. Rev. Lett.*, 2008, **100**, 125502.
10 R. Malik, D. Burch, M. Bazant and C. Gerbrand, Particle Size Dependence of the Ionic Diffusivity, *Nano Lett.*, 2010, **10**, 4123–4127.
11 C. V. Ramana, A. Mauger, F. Gendron, C. M. Julien and K. Zaghib, Study of the Li-insertion/extraction process in $LiFePO_4/FePO_4$, *J. Power Sources*, 2009, **187**, 555–564.
12 A. Andersson and J. Thomas, The source of first-cycle capacity loss in $LiFePO_4$, *J. Power Sources*, 2001, **97–8**, 498–502.
13 H. Chen, *et al.*, Carbonophosphates: A New Family of Cathode Materials for Li-Ion Batteries Identified Computationally, *Chem. Mater.*, 2012, **24**, 2009–2016.
14 C. Delmas, M. Maccario, L. Croguennec, F. Le Cras and F. Weill, Lithium deintercalation in $LiFePO_4$ nanoparticles *via* a domino-cascade model, *Nat. Mater.*, 2008, **7**, 665–671.
15 G. Chen, X. Song and T. Richardson, Electron microscopy study of the $LiFePO_4$ to $FePO_4$ phase transition, *Electrochem. Solid-State Lett.*, 2006, **9**, A295–A298.
16 J. L. Dodd, R. Yazami and B. Fultz, Phase Diagram of Li_xFePO_4, *Electrochem. Solid-State Lett.*, 2006, **9**, A151.
17 R. Malik, F. Zhou and G. Ceder, Kinetics of non-equilibrium lithium incorporation in $LiFePO_4$, *Nat. Mater.*, 2011, **10**, 587–590.
18 W. Dreyer, *et al.*, The thermodynamic origin of hysteresis in insertion batteries, *Nat. Mater.*, 2010, **9**, 448–453.
19 P. Bai, D. A. Cogswell and M. Z. Bazant, Suppression of Phase Separation in $LiFePO_4$ Nanoparticles During Battery Discharge, *Nano Lett.*, 2011, **11**, 1–7.
20 Y. Orikasa, *et al.*, Direct Observation of a Metastable Crystal Phase of Li_xFePO_4 under Electrochemical Phase Transition, *J. Am. Chem. Soc.*, 2013, **135**, 5497–5500.
21 X. Zhang, *et al.*, Rate-Induced Solubility and Suppression of the First-Order Phase Transition in Olivine $LiFePO_4$, *Nano Lett.*, 2014, **14**, 2279–2285.
22 H. Liu, *et al.*, Capturing metastable structures during high-rate cycling of $LiFePO_4$ nanoparticle electrodes, *Science*, 2014, **344**, 1252817.
23 X. Zhang, *et al.*, Direct view on the phase evolution in individual $LiFePO_4$ nanoparticles during Li-ion battery cycling, *Nat. Commun.*, 2015, **6**, 8333.
24 J. Niu, *et al.*, *In situ* observation of random solid solution zone in $LiFePO_4$ electrode, *Nano Lett.*, 2014, 1–24.
25 T. Ichitsubo, *et al.*, What determines the critical size for phase separation in $LiFePO_4$ in lithium ion batteries?, *J. Mater. Chem. A*, 2013, **1**, 14532–14537.
26 A. Abdellahi, O. Akyildiz, R. Malik, K. Thornton and C. Gerbrand, Particle-size and morphology dependence of the preferred interface orientation in $LiFePO_4$ nanoparticles, *J. Mater. Chem. A*, 2014, 15437–15447.
27 D. Morgan, A. Van der Ven and G. Ceder, Li conductivity in Li_xMPO_4 (M = Mn, Fe, Co, Ni) olivine materials, *Electrochem. Solid-State Lett.*, 2004, **7**, A30–A32.
28 J. Sugiyama, *et al.*, Magnetic and diffusive nature of $LiFePO_4$ investigated by muon spin rotation and relaxation, *Phys. Rev. B: Condens. Matter Mater. Phys.*, 2011, **84**, 054430.
29 Y. Li, *et al.*, Current-induced transition from particle-by-particle to concurrent intercalation in phase-separating battery electrodes, *Nat. Mater.*, 2014, **13**, 1149–1156.
30 G. Chen, X. Song and T. J. Richardson, Metastable Solid-Solution Phases in the $LiFePO_4/FePO_4$ System, *J. Electrochem. Soc.*, 2007, **154**, A627.
31 H. J. Tan, J. L. Dodd and B. Fultz, Thermodynamic and Kinetic Stability of the Solid Solution Phase in Nanocrystalline Li_xFePO_4, *J. Phys. Chem. C*, 2009, **113**, 20527–20530.
32 F. Zhou, K. Kang, T. Maxisch, C. Gerbrand and D. Morgan, The electronic structure and band gap of $LiFePO_4$ and $LiMnPO_4$, *Solid State Commun.*, 2004, **132**, 181–186.
33 F. Zhou, T. Maxisch and C. Gerbrand, Configurational electronic entropy and the phase diagram of mixed-valence oxides: the case of Li_xFePO_4, *Phys. Rev. Lett.*, 2006, **97**, 155704.
34 R. W. Balluffi, S. M. Allen and C. W. Carter, *Kinetics of Materials*, Wiley, 2005, p. 645.
35 H. Gabrisch, J. Wilcox and M. M. Doeff, TEM Study of Fracturing in Spherical and Plate-like $LiFePO_4$ Particles, *Electrochem. Solid-State Lett.*, 2008, **11**, A25.
36 L. Laffont, *et al.*, Study of the $LiFePO_4/FePO_4$ Two-Phase System by High-Resolution Electron Energy Loss Spectroscopy, *Chem. Mater.*, 2006, **18**, 5520–5529.
37 A. Van der Ven, A. Garikipati, S. Kim and M. Wagemaker, The Role of Coherency Strains on Phase Stability in Li_xFePO_4: Needle Crystallites Minimize Coherency Strain and Overpotential, *J. Electrochem. Soc.*, 2009, **156**, 1–9.
38 R. Malik, A. Abdellahi and G. A. Ceder, Critical Review of the Li Insertion Mechanisms in $LiFePO_4$ Electrodes, *J. Electrochem. Soc.*, 2013, **160**, A3179–A3197.
39 B. Orvananos, *et al.*, Architecture Dependence on the Dynamics of Nano-$LiFePO_4$, *Electrochim. Acta*, 2014, **137**, 245–257.
40 N. Meethong, H.-Y. S. Huang, W. C. Carter and Y.-M. Chiang, Size-Dependent Lithium Miscibility Gap in Nanoscale $Li_{1-x}FePO_4$, *Electrochem. Solid-State Lett.*, 2007, **10**, A134.
41 Y. Zhu, *et al.*, *In Situ* Atomic-Scale Imaging of Phase Boundary Migration in $FePO_4$ Microparticles During Electrochemical Lithiation, *Adv. Mater.*, 2013, **25**, 5461–5466.
42 L. Gu, *et al.*, Direct Observation of Lithium Staging in Partially Delithiated $LiFePO_4$ at Atomic Resolution, *J. Am. Chem. Soc.*, 2011, **133**, 4661–4663.
43 L. Suo, *et al.*, Highly ordered staging structural interface between $LiFePO_4$ and $FePO_4$, *Phys. Chem. Chem. Phys.*, 2012, **14**, 5363.
44 C. Zhu, *et al.*, Size-Dependent Staging and Phase Transition in $LiFePO_4/FePO_4$, *Adv. Funct. Mater.*, 2013, **24**, 312–318.
45 Y. Sun, X. Lu, R. Xiao, H. Li and X. Huang, Kinetically Controlled Lithium-Staging in Delithiated $LiFePO_4$ friven by the Fe Center Mediated Interlayer Li–Li Interactions, *Chem. Mater.*, 2012, **24**, 4693–4703.